



Unraveling the Mechanism and Kinetics of Binding of an LCI-eGFP-Polymer for Antifouling Coatings

Dominik Söder, Manuela Garay-Sarmiento, Khosrow Rahimi, Fabian Obstals, Sarah Dedisch, Tamás Haraszti, Mehdi D. Davari, Felix Jakob, Christoph Heß, Ulrich Schwaneberg, and Cesar Rodriguez-Emmenegger*

The ability of proteins to adsorb irreversibly onto surfaces opens new possibilities to functionalize biological interfaces. Herein, the mechanism and kinetics of adsorption of protein-polymer macromolecules with the ability to equip surfaces with antifouling properties are investigated. These macromolecules consist of the liquid chromatography peak I peptide from which antifouling polymer brushes are grafted using single electron transfer-living radical polymerization. Surface plasmon resonance spectroscopy reveals an adsorption mechanism that follows a Langmuir-type of binding with a strong binding affinity to gold. X-ray reflectivity supports this by proving that the binding occurs exclusively by the peptide. However, the lateral organization at the surface is directed by the cylindrical eGFP. The antifouling functionality of the unimolecular coatings is confirmed by contact with blood plasma. All coatings reduce the fouling from blood plasma by 8894% with only minor effect of the degree of polymerization for the studied range (DP between 101 and 932). The excellent antifouling properties, combined with the ease of polymerization and the straightforward coating procedure make this a very promising antifouling concept for a multiplicity of applications.

Merrill, Peppas, Andrade, Langer, and others, there have been enormous advances in biomaterials that improve healthcare, which combine advanced synthetic and natural polymers with state-of-the-art fabrication techniques.^[1–4] Such systems include passive materials aiming to perform a given function and active materials that have to integrate in the human body to perform, replace, or augment a function, such as in tissue engineering or implant technology.^[5] However, the contact of any material with the biological milieu invariably elicits unspecific interactions, which often dictate its outcome.^[6] Proteins, small molecular components of the biological media, rapidly diffuse to the foreign surface and adsorb.^[7,8] Subsequently, they act as a biological transducer that translates the presence of the surface into the language of the surrounding tissues. The ensuing adsorption of albumin, fibrinogen, or factor XII initiates uncontrolled coagulation at surfaces in contact with blood, e.g., of stents, membranes, or vascular grafts.^[9–12]

In implants it causes inflammation, which may lead to foreign body response, support of bacterial adhesion, or may promote the activation of the inflammasome with dreadful consequences such as the need of revision surgery.^[13–15] In a similar vein, protein adsorption has a deleterious effect on drug delivery


1. Introduction

With an increasingly aging population, the need for advanced medical technologies and devices, pharmaceuticals, and diagnostics is steadily increasing. Since the pioneering work from

D. Söder, M. Garay-Sarmiento, Dr. K. Rahimi, F. Obstals, S. Dedisch, Dr. T. Haraszti, Dr. F. Jakob, Prof. U. Schwaneberg, Dr. C. Rodriguez-Emmenegger
DWI – Leibniz Institute for Interactive Materials
52074 Aachen, Germany
E-mail: rodriguez@dwi.rwth-aachen.de

D. Söder, F. Obstals
Institute of Technical and Macromolecular Chemistry
RWTH Aachen University
52074 Aachen, Germany

M. Garay-Sarmiento, S. Dedisch, Dr. M. D. Davari, Dr. F. Jakob, Prof. U. Schwaneberg
Lehrstuhl für Biotechnologie
RWTH Aachen University
52074 Aachen, Germany
Prof. C. Heß
Faculty of Technology and Bionics
Rhine-Waal University of Applied Sciences
47533 Kleve, Germany

 The ORCID identification number(s) for the author(s) of this article can be found under <https://doi.org/10.1002/mabi.202100158>

© 2021 The Authors. Macromolecular Bioscience published by Wiley-VCH GmbH. This is an open access article under the terms of the Creative Commons Attribution-NonCommercial License, which permits use, distribution and reproduction in any medium, provided the original work is properly cited and is not used for commercial purposes.

DOI: 10.1002/mabi.202100158

vehicles for which the formation of a protein corona affects their stability, the ability to reach their target, or might signal their opsonization.^[16–18]

Most synthetic polymers display a rather high interfacial energy with water, e.g., $\gamma_{\text{PDMS-water}} \approx 40 \text{ mN m}^{-1}$.^[19] As proteins adsorb to minimize the interfacial energy, the minimal requirements for a surface to be antifouling is a low or zero interfacial energy with water and electroneutrality to minimize the thermodynamic drive for adsorption. However, proteins still manage to adsorb on hydrophilic surfaces by changing their conformation so that they maximize the number and strength of weak interactions between different amino acid residues and the surface.^[20,21] Several hydrophilic coatings have been designed with the aim of preventing protein adsorption, which work by creating a strong hydration layer on self-assembled monolayers,^[22–24] or entropic repulsion in hydrophilic polymers such as poly(ethylene glycol) (PEG),^[25–28] polyglycerols,^[29,30] polysaccharides,^[31,32] among others.^[33–35] However, only polymer brushes enabled complete suppression of protein adsorption.^[36–40] Polymer brushes are end-tethered polymer chains that have a stretched conformation. They provide the best repellency in water by a combination of enthalpic and entropic effects.^[25,35,41] The most significant results include the prevention of protein adsorption from diverse bodily fluids and cell adhesion.^[42,43] Polymer brushes based on oligo(ethylene glycol) methacrylate, hydroxyethyl methacrylate, phosphorylcholine methacrylate, and sulfobetaine methacrylate could reduce fouling from blood plasma by up to 90%.^[38,40] Brushes consisting of either carboxybetaines or *N*-(2-hydroxypropyl) methacrylamide (HPMA) fully prevented blood plasma protein adsorption.^[44–47] The excellent antifouling properties of the betaines have been ascribed to their ability to tightly bind and organize water molecules at their outermost interface.^[48–51] From its earliest use, poly(HPMA) found its way as an excellent bioinert polymer for drug delivery systems (macro and supramolecular) capable of extending the circulation time.^[52–56] Such effect was presumed to be related to the generation of interfaces with low protein adsorption.^[57] Later, brushes from this polymer were prepared by grafting-from approaches^[40,43,58,59] and as graft copolymers where the backbone was adsorbed onto the surface and the side poly(HPMA) chains generated the brushes.^[60] Not only did these brushes prevented protein adsorption from the most fouling bodily fluids but also created a strong repellency to bacteria. The force and work to detach a living *Yersinia pseudotuberculosis* were 60 pN and 9 aJ which correspond to 0.2% of the work necessary to detach it from Teflon.^[61] However, the excellent antifouling properties of poly(HPMA), lacking ionic moieties, must rely on a different mechanism than the betaines. Thermodynamic analysis based on the van Oss acid–base approach^[62] indicated that the Gibbs free energy of interaction between two surfaces coated with poly(HPMA) brushes across water was unfavorable ($\Delta G^{\text{hydrophobicity}} = 45.5 \text{ mJ m}^{-2} > 0$),^[63] indicating strong interaction with water in spite of lacking ionic groups. Furthermore, analysis of the components of the surface energy revealed that the polar component (γ^{AB}) was double the one of PEG-based brushes and that only a smaller fraction stemmed from the electron acceptor component (γ^+), suggesting that poly(HPMA) brushes were poor H-bond donor.^[63] Nevertheless, despite the success of these coatings, their application has not extended outside spe-

cialized labs. Their translation to medical devices demands developing strategies to bind initiators to surfaces irreversibly and requires facile processes to graft hydrophilic polymer chains directly. To date, only a limited number of works have demonstrated initiator-coupling strategies that address the broad range of surface chemistries of different materials, such as the use of plasma sputtered polymers,^[64] formation of a priming film of polydopamine,^[65–67] and the use of C–H insertion reactions.^[68,69] Moreover, the stringent polymerization conditions necessary for controlled polymerization are often too complex or expensive to translate into an industrial process. Other approaches to circumvent these difficulties include physisorption of polymers and grafting-onto via end groups or blocks. For the coatings via physisorption, polymer segments adsorb onto the substrate by weak interactions resulting in trains of loops and dangling chains. These coatings provide limited protection against protein adsorption.^[70–72] The second approach is based on linking a semi-telechelic polymer to the surface.^[27] Yet, stretched conformations are only attainable if the favorable enthalpic contribution of the binding of a single end group to the substrate overcomes the entropic cost of stretching the whole chain. Thus, this method only achieves very thin brushes and resistance to merely simple protein solutions has been reported.^[25,28,39,73,74]

Recently, we introduced a new concept for antifouling coatings based on fully hydrophilic macromolecules that do not form aggregates in water while the presence of an interface leads to selective adsorption of one block and the segregation of the second block to generate a brush-like antifouling structure.^[75] The key challenge was to design a surface-affine block that adsorbs at interfaces to minimize the interfacial energy, like a macromolecular amphiphile, but in the absence of the surface, it is fully dissolved and does not form any supramolecular aggregates, which would pose as a kinetic barrier to adsorption. Proteins and peptides are particularly well-suited for this as they are molecularly dissolved in water while the presence of an interface alters the balance of intramolecular/solvent interactions, enabling to change conformation and to selectively expose amino acid residues and maximize the adsorption to virtually any surface.^[3] For this, the surface-affine grafting block was built by the genetic fusion of the antimicrobial amphiphilic liquid chromatography peak I (LCI) peptide with the enhanced green fluorescent protein (eGFP). LCI derives from *Bacillus subtilis*, consists of 47 amino acids, and comprises four antiparallel β -sheets that confer high thermal stability.^[76] By means of the different amino acids, LCI is capable of exerting a multiplicity of weak interactions (H-bonding, hydrophobic effect, ionic interactions) that drive its physisorption from aqueous dilute solutions onto highly diverse surfaces including cyclic olefin copolymer, polytetrafluoroethylene, titanium, hair, teeth, leaves,^[75,77,78] as well as polystyrene, polypropylene, stainless steel, gold, and silicon wafer.^[79–83] The antifouling block was based on a hydrophilic polymer (pHPMA) grafted via single electron transfer-living radical polymerization (SET-LRP)^[84–90] directly from an initiator linked to a cysteine residue in the eGFP.

But does the adsorption proceed exclusively by LCI or by a combination of mechanisms? And what is the role of eGFP and of the degree of polymerization (DP) in the formation of antifouling coatings? To unravel the mechanism of binding, we synthesized LCI-eGFP-pHPMA with varying DP by SET-LRP and studied

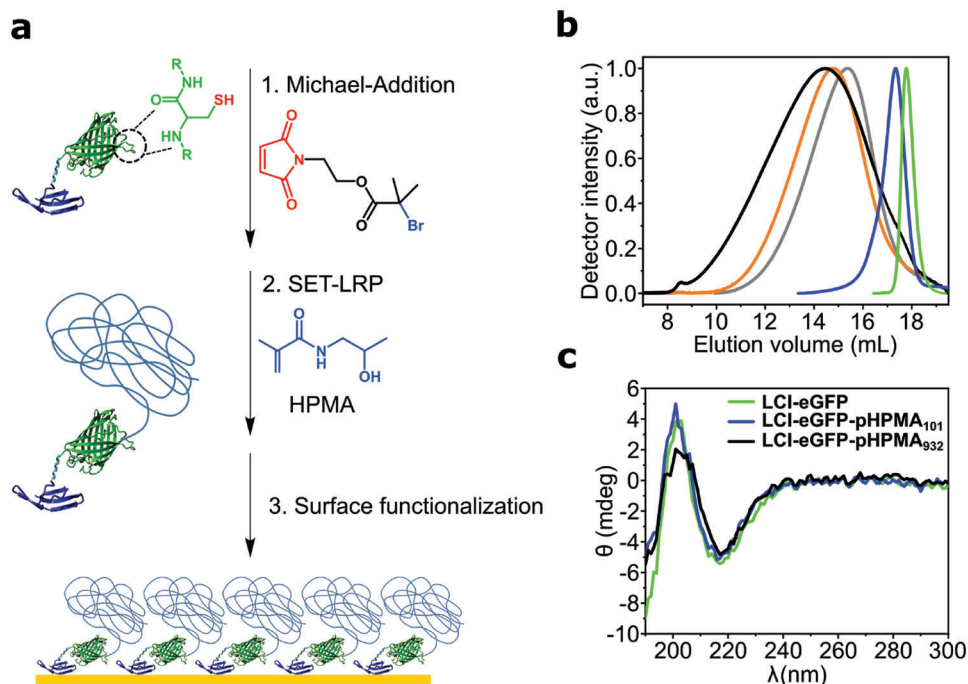


Figure 1. a) Linkage of the maleimide initiator to the cysteine residue of eGFP, followed by grafting of poly(HPMA) using SET-LRP and the oriented adsorption process to surfaces. b) SEC of the bare protein (green) and LCI-eGFP-pHPMA with DPs of 101 (blue), 699 (gray), 843 (orange), and 932 (black). c) CD spectra of LCI-eGFP (green) and LCI-eGFP-pHPMA with a DP of 101 (blue) and 932 (black).

their assembly on gold. By utilizing X-ray reflectivity (XRR) and atomic force microscopy (AFM), we investigated the organization of the LCI-eGFP-pHPMA. By a multilayer fitting we analyzed the thickness, roughness, and scattering length density of every component (three layers) and studied the influence of the DP and grafting density. Lastly, surface plasmon resonance (SPR) spectroscopy measurements demonstrated the dependency of the DP and the surface grafting density on the antifouling capabilities against the adsorption of blood plasma proteins.

2. Results and Discussion

2.1. Synthesis of LCI-eGFP-pHPMA Macromolecules

The macroinitiator was synthesized by conjugating one maleimide-initiator to the free cysteine of LCI-eGFP (eGFP, position 69)^[75,91] via a thiol-maleimide Michael addition (Figure 1a). Poly(HPMA) was directly grafted from LCI-eGFP-initiator in phosphate-buffered saline (PBS) buffer at room temperature using SET-LRP. We selected SET-LRP because it accounts for very fast kinetics and control even for methacrylamide monomers in aqueous media with minimal bimolecular termination.^[89,90,92] The latter is necessary to prevent dimer formation that would obscure the adsorption process, whereas the compatibility with water is necessary to maintain the integrity of the proteins. The polymerization was performed using a hydrazine-activated copper wire as catalyst,^[93] the LCI-eGFP-initiator, and the following ratios of [Monomer]:[CuBr₂]:[Me₆TREN]:[LCI-eGFP-initiator] = [X]:[0.1]:[0.6]:[1], where X represents the molar ratio of monomer ranging from 300 to 800 (Table S1, Supporting Information). We performed the polymerization at different monomer to

initiator ratios to have a broad variation in the DP (Table S1, Supporting Information). Hereafter, the samples are referred to as LCI-eGFP-pHPMA_x, where X corresponds to number average DP calculated from M_n obtained from size exclusion chromatography (SEC) in PBS. All polymerizations afforded polymers as confirmed by ¹H NMR (Supporting Information, Figure S1). SEC revealed molecules with monomodal distribution of molecular weight and no presence of free initiator (Figure 1b), indicating a quantitative initiation efficiency, well in line with previous reports for aqueous SET-LRP.^[92,94] The molecular weight distribution increased with the monomer-to-initiator ratio and with conversion. The M_n were well beyond LCI-eGFP ranging from 51,430 to 170,420 g mol⁻¹, which correspond to DPs from 101 to 932 (Figure 1b and Table S1, Supporting Information). Some broadening of the molecular weight distribution was observed for the sample LCI-eGFP-pHPMA₉₃₂, however it remained monomodal. Thus, the polymerization condition allowed the polymerization of very large molecular weights even in aqueous medium.

Circular dichroism (CD) spectroscopy was performed for the LCI-eGFP-pHPMAs to assess whether the secondary structure of the peptide was affected by grafting high molecular weight polymers. Figure 1c shows positive (200 nm) and negative bands (218 nm) corresponding to four antiparallel β -sheets of LCI and 11 β -sheets of eGFP which remained unchanged after polymerization. Thus, CD confirmed that the secondary structure of LCI-eGFP remained unaltered even by grafting polymers of tenfold size. This could also be inferred by the unmodified fluorescence stemming from the eGFP structure.

An important part of the concept is that the LCI-eGFP-pHPMAs remain molecularly dissolved, as aggregates would

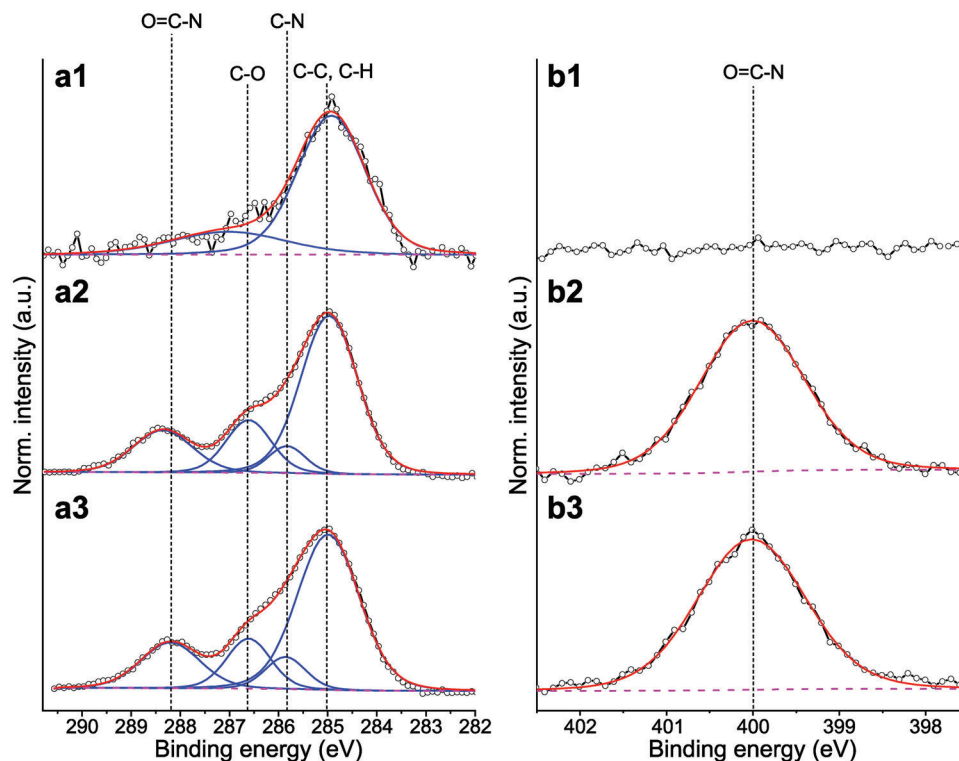


Figure 2. High-resolution C1s (left) and N1s (right) XPS spectra of surface modifications on gold; a1/b1 = bare gold, a2/b2 = LCI-eGFP, a3/b3 = LCI-eGFP-pHPMA₄₉₁.

pose kinetic barriers to adsorption. Dynamic light scattering (DLS) measurements showed that LCI-eGFP displayed a hydrodynamic diameter of 5.3 nm. Grafting poly(HPMA) from it resulted in a gradual increase of the hydrodynamic radius from 6.2 to 18.7 nm (Figure S2 and Table S2, Supporting Information). No aggregates could be observed in the intensity, volume, and number distributions of hydrodynamic radii. Thus, DLS measurements demonstrate that the LCI-eGFP-pHPMAs do not form supramolecular aggregates in water.

2.2. Formation of LCI-eGFP-pHPMA Film on Gold

The coating was assembled on gold by the molecular physisorption of LCI-eGFP-pHPMA. PBS solutions of the macromolecules were contacted with gold-coated silicon wafers for 60 min, followed by copious rinsing with PBS and ultrapure water. The resulting films had a thickness of about 5 nm by ellipsometry, suggesting that the coatings were only one molecule thick. Additionally, AFM of the LCI-eGFP-pHPMA coatings revealed an ultrathin film that followed the facets of the polycrystalline gold substrate (Figure S3, Supporting Information).

The chemical composition of the coatings was confirmed using X-ray photoelectron spectroscopy (XPS). **Figure 2** depicts the high-resolution C1s (a) and N1s (b) spectra of a bare gold surface and gold surfaces after functionalization with LCI-eGFP and LCI-eGFP-pHPMA₄₉₁ via physisorption at a concentration of 400 $\mu\text{g mL}^{-1}$. The presence of adventitious carbon adsorbed from the atmosphere could be observed on the C1s spectrum of bare gold

(a1) depicting signals characteristic of C–C, C–H at 285.0 eV and C–O around 286.6 eV. No nitrogen was observed in the N1s spectrum. It is of note that the amount of counts in the C1s is 5–10 times lower on gold than on any of the coated surfaces.

After adsorption of LCI-eGFP and the LCI-eGFP-pHPMA, the C1s spectra (a2 and a3) revealed new signals at 285.8 and 286.6 eV, corresponding to the signals of C–N and C–O, respectively.^[47] The presence of these signals correlates with the chemical structures of the protein and HPMA. Importantly, the peak at 288.2 eV indicates a strong presence of amide bonds, which can be ascribed to the peptide bonds in the protein and the methacrylamide backbone of poly(HPMA). In contrary to the bare gold surface (b1), the high-resolution N1s spectra of the functionalized samples (b2 and b3) clearly show a component at 400 eV, stemming from amide bonds.^[95]

2.3. Unraveling the Mechanism of LCI-eGFP-pHPMA Binding and Film Formation

To elucidate the mechanism of binding of LCI-eGFP-pHPMA on gold, we determined the adsorption isotherms and electron density profiles. For the studies of binding kinetics, we utilized LCI-eGFP-pHPMA₄₉₁, as it exhibits a narrow molecular weight distribution (homogeneity of sizes), while providing a molecular weight significantly higher than LCI-eGFP. We quantified the surface adsorption of LCI-eGFP-pHPMA₄₉₁ at different concentrations (0.04–1000 $\mu\text{g mL}^{-1}$, 0.37×10^{-9} to 9.33×10^{-6} M) by SPR. Here, the change in baseline refractive index before and

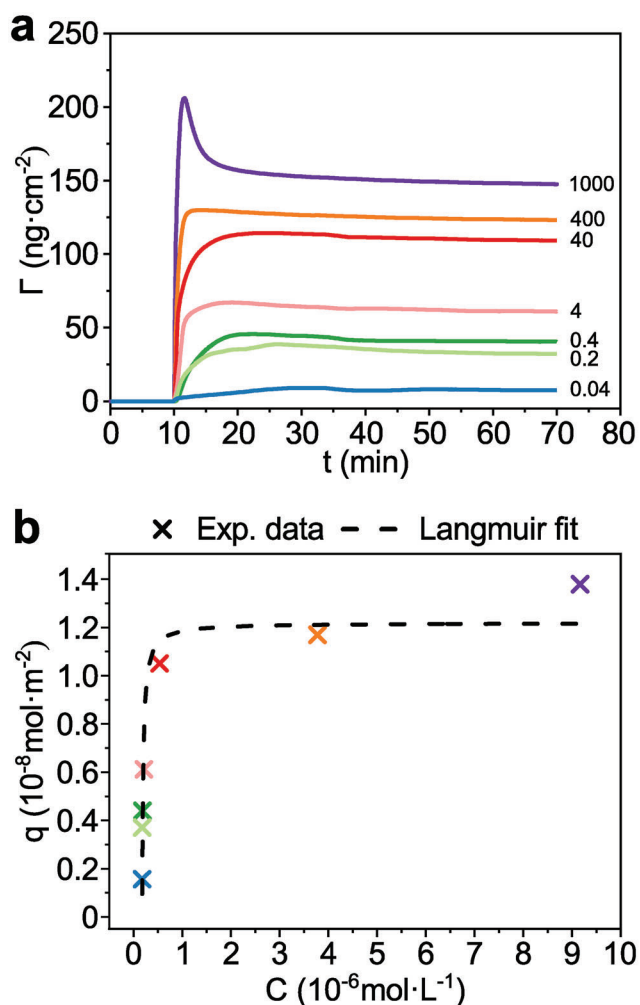


Figure 3. a) Binding of LCI-eGFP-pHPMA₄₉₁ at different concentrations on gold as obtained by SPR. Sensograms were obtained at a flow rate of $10\ \mu\text{L}\ \text{min}^{-1}$ and are labeled with the sample concentrations in $\mu\text{g mL}^{-1}$. b) Surface coverage values (crosses) as obtained from (a). The dashed line represents the Langmuir fit of the experimental isotherm.

after injection is proportional to the mass adsorbed to the surface (Figure 3a, see Supporting Information for calculation and Table S3). Comparison of all data plots (Figure 3b, crosses) illustrates a fast-initial increase in mass adsorbed with higher sample concentrations, until $400\ \mu\text{g mL}^{-1}$ ($3.73 \times 10^{-6}\ \text{M}$) and thereafter a plateau is observed. The adsorption isotherm could be fitted with a Langmuir-like profile (Equation (1), see the Supporting Information for derivation)^[96]

$$q = \frac{QC}{C + K_{\text{eq}}} \quad (1)$$

where Q is the amount of solute attached at surface saturation and q is the amount of solute at the surface for a given concentration (C) with K_{eq} being the adsorption equilibrium constant. This model relies on the following assumptions: 1) the sample saturates as a monolayer; 2) the surface consists of homogenous adsorption sites available for one type of adsorbate; and 3) a

dynamic equilibrium of adsorption and desorption is achieved in the course of the experiment.^[96,97] Such model could be fitted only if one type of adsorbate was present, suggesting that LCI preferentially binds the surface compared to poly(HPMA) part. However, eGFP may also adsorb. Thus, control experiments monitoring the kinetics of eGFP binding to gold were carried out demonstrating that the affinity of the eGFP was much lower than the one of LCI (Supporting Information, Figure S5). Thus, LCI governs the binding process. The values K_{eq} and Q can be determined by fitting Equation (1). By fitting Equation (1) to an isotherm plot of q (in mol m^{-2}) versus C (in mol L^{-1}) (Figure 3b), one can determine K_{eq} , Q , and the Gibbs free energy of adsorption G_{ads} . The average K_{eq} is $3.75 \times 10^7\ \text{L mol}^{-1}$, resulting in an average ΔG_{ads} of $-10.22\ \text{kcal mol}^{-1}$ ($-42.78\ \text{kJ mol}^{-1}$, see the Supporting Information), a promising adsorption strength when compared to the interaction of biotin and avidin, one of the strongest noncovalent binding in nature with a $\Delta G_{\text{binding}}$ of $-20.4\ \text{kcal mol}^{-1}$.^[98] From Q , we derived a maximal obtainable surface mass of $128\ \text{ng cm}^{-2}$ ($1.19\ \text{pmol cm}^{-2}$). It is worth noting that a similar amount of protein adsorption is observed when bare gold is contacted with a model protein like serum albumin $\Gamma_{\text{albumin}} = 126\ \text{ng cm}^{-2}$.^[64] The Langmuir-type adsorption isotherm indicates a single mode of binding, i.e., the LCI-eGFP-pHPMA must adsorb using the same part of the macromolecule, which was assumed to be the LCI. To assess the validity of our hypothesis, we studied the grafting density and electron density of the films using XRR. This method provides information on the thickness, roughness, as well as the electron density profile of the thin film along the surface normal. XRR was performed on gold-coated silicon wafers for different surface coatings consisting of bare LCI-eGFP and LCI-eGFP-pHPMA of different molecular weights. After fitting (Figure S7, Supporting Information), the experimental data were simulated using the parrot formalism.^[99] The modeling of the film was performed using a multi-slab model with separated SiO_2 , TiO_2 , Au, LCI, eGFP, and poly(HPMA) layers. The scattering length densities (SLD), thickness, and roughness for each sample computed from the fit parameters are shown in Figure 4b,c,e,g and summarized in Table S5 in the Supporting Information.

First, we analyzed the coating of LCI-eGFP (no polymer) which was modeled as a film with two slabs. The first slab (I) was positioned at the interface with Au, while the second (II) at the interface with air. The fitting resulted in a thickness of $1.9\ \text{nm}$ for slab (I) and $4.8\ \text{nm}$ for slab (II), close to the height of eGFP ($4.2\ \text{nm}$), with an SLD of 0.6 and $1.4 \times 10^{-5}\ \text{\AA}^{-2}$, respectively. The height of the slab I is in close agreement with the height of an LCI peptide fully spread calculated using molecular modeling with YASARA (Supporting Information, Figure S6 and Table S4). Furthermore, the XRR data suggest that the top layer consists of eGFP that are packed with their axis preferably orthogonal to the surface. Therefore, in this model slab (I) should consist of LCI and its linker, an α -helix (17 amino acids).^[75] Figure 4d illustrates a model for the assembly of LCI-eGFP consistent with the XRR. Geometrical analysis of eGFP and LCI indicates that their cross-sections are similar; 4.5 and $4.0\ \text{nm}^2$, respectively.^[80] However, there are striking differences in the SLD of both slabs despite the peptides mainly consisting of β -sheets and α -helix (from the linker) of similar density. The dimensions of slab (II) are consistent with the packing of eGFP presumably driven by lateral

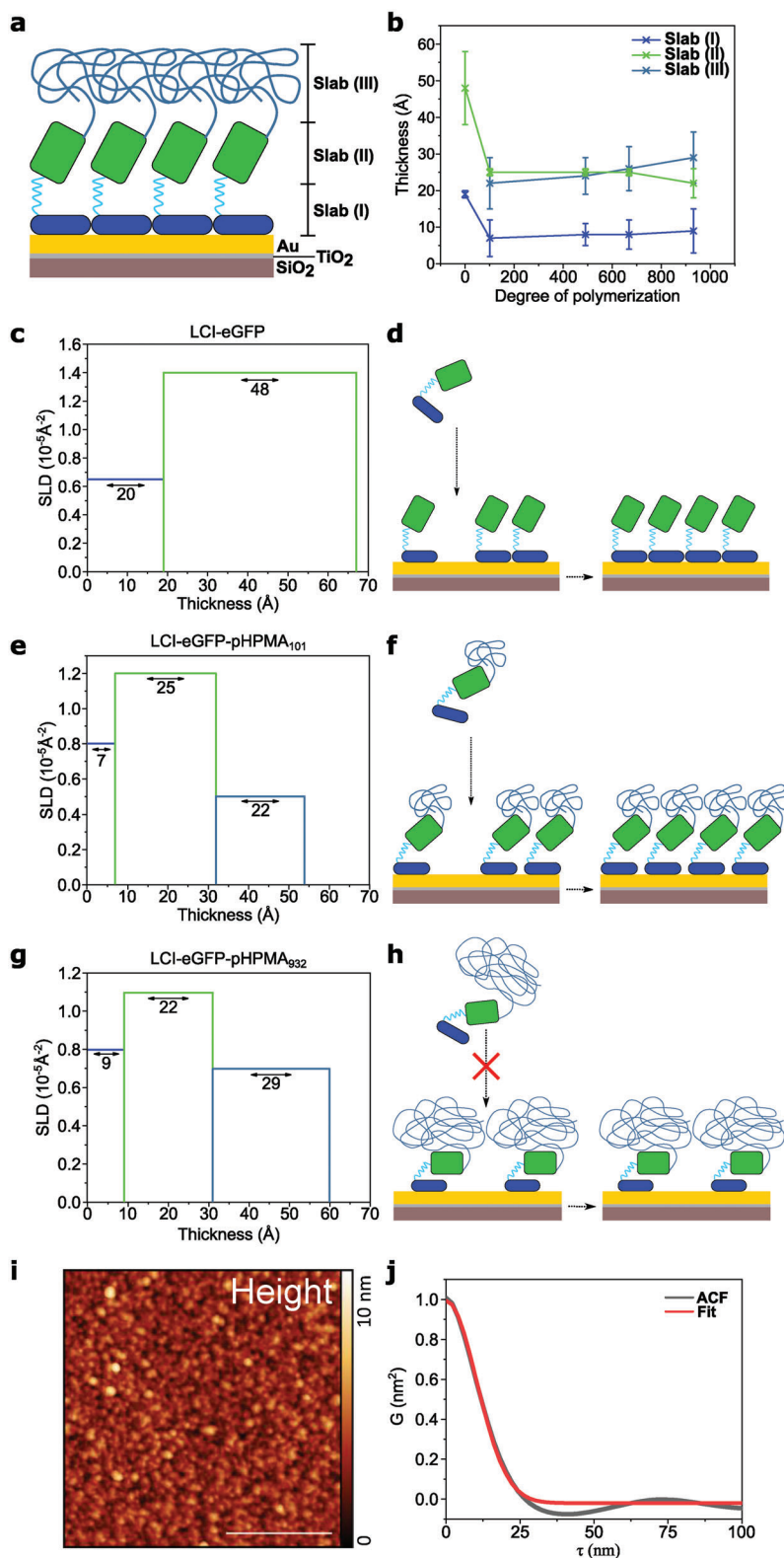


Figure 4. a) Sketch of layers of the modeled multi-slab surface film. b) Thickness of slab (I), (II), and (III) as a function of DP. c) SLD and thickness of slab (I) and (II) of LCI-eGFP. d) Scheme of surface adsorption of LCI-eGFP on gold. e) SLD and thickness of slab (I), (II), and (III) of LCI-eGFP-pHPMA₁₀₁. f) Scheme of surface adsorption of LCI-eGFP-pHPMA with low DP. g) SLD and thickness of slab (I), (II), and (III) of LCI-eGFP-pHPMA₉₃₂. h) Scheme of surface adsorption of LCI-eGFP-pHPMA with high DP. i) AFM height image of LCI-eGFP-pHPMA₉₃₂ on mica, scale bar is 400 nm. j) 1D ACF of the surface topography with a Gaussian function fit.

associations. However, the thickness of slab (I) is higher than the molecular thickness of LCI indicating that the resulting SLD is the combination of the SLD of LCI and peptide linker—which is orthogonal to the surface—and of air. This model suggests that the assembly is driven by LCI but once on the surface lateral interactions between eGFP determine the maximum density.

Grafting poly(HPMA) from LCI-eGFP had a clear effect in the assembly. A third slab (III) was necessary to account for poly(HPMA). The thickness of slab (III) increased with the increment of the degree of polymerization while the SLD remains constant. However, the bulky size of the polymer caused differences in the slab beneath. Even the polymer with the smallest degree of polymerization resulted in a marked decrease in the thickness from 48 to 25 Å and a reduction of the SLD from 1.4 to 1.2. Increasing the degree of polymerization from 101 to 669 did not result in changes in the thickness of slab (II) nor the SLD. This suggests that there was no increase in the separation between the eGFP at that range of degree of polymerization. But how can slab (II) maintain the same SLD when the steric repulsion between the poly(HPMA) top groups aim at forcing it apart? We hypothesize that tilting of eGFP can account for the need of a larger interface area with poly(HPMA) and for the observed decrease in thickness between the LCI-eGFP and LCI-eGFP-pHPMA (Figure 4f,h). The tilting of eGFP requires strong tipping of the rigid peptide linker. This is reflected in the lower thickness and corresponding higher SLD of slab (I) in the presence of poly(HPMA).

Furthermore, we utilized AFM to assess how LCI-eGFP-pHPMA arranged when confined to an interface, at the surface of mica. In these studies, we utilized mica to rule out the effect of the roughness of the substrate. The topographic images evidenced that the LCI-eGFP-pHPMA coating consisted of granules packed without pinholes (Figure 4i,j). To estimate the granule size, we used a 1D autocorrelation function (ACF), which was calculated along the fast scanning axis and was averaged for all lines. The ACF was then fitted to a Gaussian function to obtain the average radius of an equivalent disk that has the same projected area than the granules. The obtained radii for LCI-eGFP-pHPMA₉₃₂ were 14.5 nm ± 0.25 nm (Supporting Information, Figure S4). Such average radius was larger than the hydrodynamic radius (9 nm) measured for the same molecule by DLS. This indicates that upon adsorption the poly(HPMA) part of the molecule spreads at the interface increasing the interfacial area while decreasing the height, well in line with the XRR observation and model (Figure 4h).

2.4. Influence of Degree of Polymerization and Grafting Density on Antifouling Capabilities

We studied the antifouling capabilities utilizing coatings prepared from LCI-eGFP-pHPMA with varying DP as well as different surface densities and evaluated their resistance to protein fouling from blood plasma with SPR. Protein adsorption from blood plasma (10% in PBS) was measured after surface saturation with the LCI-eGFP-pHPMA solutions was achieved. The difference in sensor response (detected as $\Delta\mu RIU$) between baselines before and after injection is proportional to the mass adsorbed on the surface (see Supporting Information for calculation and Figure S8).

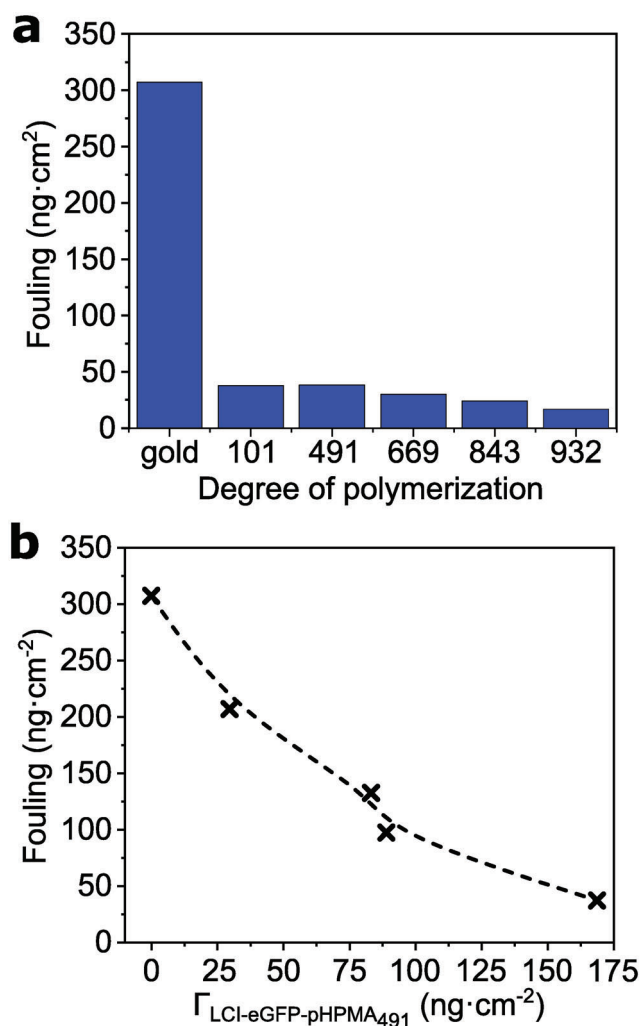


Figure 5. a) Fouling of 10% blood plasma on bare gold and on surfaces coated with LCI-eGFP-pHPMA with increasing DP. b) The reduction of fouling of 10% blood plasma for LCI-eGFP-pHPMA₄₉₁ at different surface densities.

We analyzed the effect of the DP on the antifouling behavior at a concentration of 2400 μg mL⁻¹, and compared the fouling of blood plasma on gold before and after coating with LCI-eGFP-pHPMA (Figure 5a). Even the sample having the lowest DP already reduced the fouling by 88% (38 ng cm⁻²). Slight improvements were observed by increasing DP in the range of 669–932 to reach a decrease in fouling by 94% (17 ng cm⁻²). The values of fouling are almost on par to those of best polymer brushes^[40,58,100,101] and much lower than for other hydrophilic coatings based on grafted linear^[39,102] or star-shaped^[103] polymers, hydrogels^[104] and even four orders of magnitude lower than microgels.^[105]

Additionally, we investigated the antifouling properties in regards of the surface density. We systematically varied the surface density of LCI-eGFP-pHPMA₄₉₁ and assessed the fouling from 10% blood plasma. Figure 5b shows that increasing the grafting density from 30 to 170 ng cm⁻² results in a drastic reduction of adsorbed proteins, highlighting the importance of the close

arrangement of the LCI-eGFP. Interestingly, surface densities as low as 89 ng cm^{-2} (formed from a solution $c = 400 \text{ } \mu\text{g mL}^{-1}$) were already sufficient to fully prevent adsorption of albumin and to decrease blood plasma fouling to 98 ng cm^{-2} which is equivalent to a reduction of 68% of fouling on gold. On the other hand, after achieving complete surface saturation (168 ng cm^{-2}), only 20 ng cm^{-2} of blood plasma could be detected. Such level is in pair with the best antifouling polymer brushes.^[39,40,43,44,58]

3. Conclusion

We studied the adsorption and assembly of peptide-polymer macromolecules for universal antifouling surface functionalization based on LCI-eGFP. Adsorption isotherms of LCI-eGFP-pHPMA determined by SPR followed a Langmuir-type behavior, indicating that the adsorption was driven by a single part of the LCI-eGFP-pHPMA molecule, i.e., oriented immobilization. XRR and AFM measurements confirmed that the binding occurs solely by the LCI-peptide. However, it also demonstrated that the packing of the cylindrical eGFPs controls the assembly at the gold surface. The grafting of LCI-eGFP-pHPMA results in eGFP tilted from the normal to the surface. The tilt increases with the DP of poly(HPMA). This allows for a larger interface between eGFP and poly(HPMA) without reducing the attractive interactions between LCI-surface and the packing of eGFPs.

The formed coatings displayed antifouling properties on par with the best polymer brushes grafted from surface. Only minor changes in the repulsion to proteins were observed for the DPs evaluated, however, a pronounced deterioration of the antifouling efficacy was observed when the density of the LCI-eGFP-pHPMA was decreased away from the equilibrium saturation.

Interestingly, concentrations as low as $400 \text{ } \mu\text{g mL}^{-1}$ (89 ng cm^{-2}) were already sufficient to fully prevent adsorption of albumin and to decrease blood plasma fouling to 98 ng cm^{-2} which is equivalent to a reduction of 68% of fouling. Further increase of solution concentration to $2400 \text{ } \mu\text{g mL}^{-1}$ (168 ng cm^{-2}) allowed to obtain surface saturation and excellent antifouling properties, paving the way to the translation of this technology to the medical field.

4. Experimental Section

Further details on procedures and instrumentation are given in the Supporting Information.

Chemicals and Materials: All chemicals were analytical purity and were used as received unless stated otherwise. LCI-eGFP was produced in *E. coli* and purified as previously described (details can be found in the Supporting Information).^[80]

Synthesis of LCI-eGFP-pHPMA via SET-LRP: HPMA (see Table S1, Supporting Information), PBS (0.5 mL), CuBr₂ (9.8 μg , 29.3 μmol , 0.1 eq.), ME6TREN (30 μL , 170 μmol , 0.6 eq.), and protein-initiator solution (1 mL, 0.38 mol, 1 eq.) were added to a 10 mL Schlenk tube. Subsequently, a hydrazine-activated copper wire (4.5 cm x 0.1 cm) wrapped around a magnetic stir bar was added to the Schlenk flask and kept out of the liquid with a magnet. The solution was degassed by at least five freeze-pump-thaw cycles. The reaction was initiated by dropping the Cu-wire into the solution at 28 °C and allowed to proceed for 18–20 h. The samples were purified by using centrifugal filter units (Amicon Ultra-15, 10 kDa cut-off, Merck Millipore Ltd.) and two washing steps.

Adsorption Kinetics by SPR: Sensor slides (gold coated, Cenibra, Germany) were pre-cleaned by rinsing with absolute ethanol and ultra-pure water. Adsorption kinetics were monitored using the MP-SPR Navi 210A VASA (BioNavis, Finland) by injecting a solution of LCI-eGFP-pHPMA₄₉₁ at concentrations of 1000, 400, 40, 20, 4, 0.4, 0.2, and $0.04 \text{ } \mu\text{g mL}^{-1}$ in PBS at a flow rate of $10 \text{ } \mu\text{L min}^{-1}$ for 25 min, followed by flow of PBS at $10 \text{ } \mu\text{L min}^{-1}$ until a stable baseline was reached. To evaluate the results, SPR-Navi Data Viewer (Version 4.3.5.2) was used. Measurements results at 670 nm were used for data comparison and analysis. Adsorption isotherms were built from the obtained values of equilibrium adsorption.

Formation of Monomolecular Coatings of LCI-eGFP-pHPMA on Gold: Gold-coated silica wafers were cut into pieces of 2 cm^2 and rinsed twice with pure ethanol and ultrapure water. The coating was carried out by immersing the wafers in a solution of LCI-eGFP-pHPMA ($400 \text{ } \mu\text{g mL}^{-1}$) in PBS for 1 h. Subsequently, the solution was diluted by adding and removing $5 \times 1 \text{ mL}$ of PBS and $2 \times 1 \text{ mL}$ ultrapure water. The samples were stored in ultrapure water and were dried just before use. These samples were utilized for ellipsometry, XRR, and XPS analysis.

Determination of Density of Monomolecular Coatings of LCI-eGFP-pHPMA by XRR: Gold-coated silicon wafers were covered with LCI-eGFP as well as LCI-eGFP-pHPMA with DPs of 101, 491, 669, and 932 as described above. XRR measurements were performed using an Empyrean setup from PANalytical with a Cu X-ray tube (line source of $12 \times 0.04 \text{ mm}^2$) providing Cu K α radiation with $\lambda = 0.1542 \text{ nm}$. A divergence slit of $1/32^\circ$ was set to illuminate part of the parabolic graded multilayer system (Göbel mirror), while the latter was converted 0.8° from the divergent beam into an almost parallel beam (divergence $\leq 55 \text{ mdeg}$). This geometry was used to improve the measurement at low angles. On the diffraction side, a receiving slit, 0.04 Soller slit, and PANalytical pixel detector (256×256 pixels of $55 \text{ } \mu\text{m}$) were used to collect the scattered signals. The setup was calibrated using a high-quality Si-wafer, which resulted in 26 mdeg resolution. X'Pert reflectivity software was used for the fitting process, whereas Parratt32 (Version 1.6.0) was used for electron density profiling.

Protein Adsorption on LCI-eGFP-pHPMA Coatings: Unspecific protein adsorption was measured by flowing blood plasma (10% in PBS) over LCI-eGFP-pHPMA coatings at a flow rate of $6 \text{ } \mu\text{L min}^{-1}$ while monitoring the resonant angle in SR7500DC SPR (Reichert Technologies, USA). The coatings were formed in situ by flowing a solution of LCI-eGFP-pHPMA at a concentration of $2400 \text{ } \mu\text{g mL}^{-1}$ in PBS at a flow rate of $6.0 \text{ } \mu\text{L min}^{-1}$ until equilibrium was reached, followed by PBS washing until a stable baseline was acquired. Immediately afterward, a 10% blood plasma solution was flowed until equilibration, followed by a final PBS washing step until a stable baseline was again discernible. To assess the effect of the grafting density in the antifouling properties, LCI-eGFP-pHPMA₄₉₁ coatings were formed at different concentrations (2400, 400, 4, and $0.04 \text{ } \mu\text{g mL}^{-1}$) and fouling was determined as described above.

Supporting Information

Supporting Information is available from the Wiley Online Library or from the author.

Acknowledgements

The authors thank the support of the research association of Forschungskuratorium Textil e.V. supported via AiF ("Arbeitsgemeinschaft Industrielle Forschungsvereinigungen Otto von Guericke e.V."), research project IGF-No. 19893 N within the promotion program of "Industrielle Gemeinschaftsforschung" (IGF) of the Federal Ministry for Economic Affairs and Energy on the basis of a decision by the German Bundestag. This work was also partially performed at the Center for Chemical Polymer Technology CPT, which was supported by the EU and the federal state of North Rhine-Westphalia (grant EFRE 30 00 883 02). Table of content figure was partially created with BioRender.com

Open access funding enabled and organized by Projekt DEAL.

Conflict of Interest

The authors declare no conflict of interest.

Data Availability Statement

Data available on request from the authors.

Keywords

adhesion peptides, antifouling, aqueous SET-LRP, biomimetic coating, surface functionalization

Received: April 16, 2021

Revised: May 15, 2021

Published online: June 18, 2021

- [1] N. A. Peppas, E. W. Merrill, *J. Biomed. Mater. Res.* **1977**, *11*, 423.
- [2] N. A. Peppas, R. Langer, *Science* **1994**, *263*, 1715.
- [3] J. D. Andrade, *Surface and Interfacial Aspects of Biomedical Polymers*, Springer, Boston, MA **1985**.
- [4] R. Langer, D. A. Tirrell, *Nature* **2004**, *428*, 487.
- [5] F. M. Chen, X. Liu, *Prog. Polym. Sci.* **2016**, *53*, 86.
- [6] D. F. Williams, *Biomaterials* **2009**, *30*, 5897.
- [7] L. Vroman, A. L. Adams, *J. Biomed. Mater. Res.* **1969**, *3*, 43.
- [8] L. Vroman, A. L. Adams, in *Proteins at Interfaces*, Vol. 343 (Eds: T. A. Horbett, J. Brash), ACS Publications, Washington **1987**, Ch. 10.
- [9] S. de Maat, C. Maas, *J. Thromb. Haemostasis* **2016**, *14*, 1498.
- [10] B. Sivaraman, R. A. Latour, *Biomaterials* **2010**, *31*, 1036.
- [11] B. Sivaraman, R. A. Latour, *Biomaterials* **2010**, *31*, 832.
- [12] B. D. Ratner, A. S. Hoffman, F. J. Schoen, J. E. Lemons, *Biomaterials Science: An Introduction to Materials in Medicine*, Elsevier, New York **2004**.
- [13] J. M. Anderson, *Annu. Rev. Mater. Res.* **2001**, *31*, 81.
- [14] D. Pavithra, M. Doble, *Biomed. Mater.* **2008**, *3*, 034003.
- [15] R. Maitra, C. C. Clement, B. Scharf, G. M. Crisi, S. Chitta, D. Paget, P. E. Purdue, N. Cobelli, L. Santambrogio, *Mol. Immunol.* **2009**, *47*, 175.
- [16] S. Behzadi, V. Serpooshan, R. Sakhtianchi, B. Muller, K. Landfester, D. Crespy, M. Mahmoudi, *Colloids Surf., B* **2014**, *123*, 143.
- [17] S. Ritz, S. Schottler, N. Kotman, G. Baier, A. Musyanovych, J. Kuharev, K. Landfester, H. Schild, O. Jahn, S. Tenzer, V. Mailander, *Biomacromolecules* **2015**, *16*, 1311.
- [18] G. Settanni, J. Zhou, T. Suo, S. Schottler, K. Landfester, F. Schmid, V. Mailander, *Nanoscale* **2017**, *9*, 2138.
- [19] H. W. Fox, P. W. Taylor, W. A. Zisman, *Ind. Eng. Chem.* **1947**, *39*, 1401.
- [20] T. McPherson, A. Kidane, I. Szeifer, K. Park, *Langmuir* **1998**, *14*, 176.
- [21] A. Halperin, *Langmuir* **1999**, *15*, 2525.
- [22] Y. Y. Luk, M. Kato, M. Mrksich, *Langmuir* **2000**, *16*, 9604.
- [23] R. L. C. Wang, H. J. Kreuzer, M. Grunze, *J. Phys. Chem. B* **1997**, *101*, 9767.
- [24] R. E. Holmlin, X. X. Chen, R. G. Chapman, S. Takayama, G. M. Whitesides, *Langmuir* **2001**, *17*, 2841.
- [25] S. I. Jeon, J. H. Lee, J. D. Andrade, P. G. De Gennes, *J. Colloid Interface Sci.* **1991**, *142*, 149.
- [26] L. D. Unsworth, H. Sheardown, J. L. Brash, *Biomaterials* **2005**, *26*, 5927.
- [27] L. D. Unsworth, H. Sheardown, J. L. Brash, *Langmuir* **2005**, *21*, 1036.
- [28] L. D. Unsworth, H. Sheardown, J. L. Brash, *Langmuir* **2008**, *24*, 1924.
- [29] R. K. Kainthan, M. Gnanamani, M. Ganguli, T. Ghosh, D. E. Brooks, S. Maiti, J. N. Kizhakkedathu, *Biomaterials* **2006**, *27*, 5377.
- [30] M. Wyszogrodzka, R. Haag, *Biomacromolecules* **2009**, *10*, 1043.
- [31] M. Morra, C. Cassinelli, *J. Biomater. Sci., Polym. Ed.* **1999**, *10*, 1107.
- [32] S. L. McArthur, K. M. McLean, P. Kingshott, H. A. W. St John, R. C. Chatelier, H. J. Griesser, *Colloids Surf., B* **2000**, *17*, 37.
- [33] D. Xiao, H. Zhang, M. Wirth, *Langmuir* **2002**, *18*, 9971.
- [34] Y. Mei, T. Wu, C. Xu, K. J. Langenbach, J. T. Elliott, B. D. Vogt, K. L. Beers, E. J. Amis, N. R. Washburn, *Langmuir* **2005**, *21*, 12309.
- [35] R. Barbey, L. Lavanant, D. Paripovic, N. Schuwer, C. Sugnaux, S. Tugulu, H. A. Klok, *Chem. Rev.* **2009**, *109*, 5437.
- [36] Y. Chang, S. Chen, Z. Zhang, S. Jiang, *Langmuir* **2006**, *22*, 2222.
- [37] S. Chen, L. Liu, S. Jiang, *Langmuir* **2006**, *22*, 2418.
- [38] Z. Zhang, T. Chao, S. Chen, S. Jiang, *Langmuir* **2006**, *22*, 10072.
- [39] C. Rodriguez-Emmenegger, E. Brynda, T. Riedel, Z. Sedlakova, M. Houska, A. B. Alles, *Langmuir* **2009**, *25*, 6328.
- [40] C. Rodriguez-Emmenegger, E. Brynda, T. Riedel, M. Houska, V. Subr, A. B. Alles, E. Hasan, J. E. Gautrot, W. T. Huck, *Macromol. Rapid Commun.* **2011**, *32*, 952.
- [41] L. Li, S. Chen, J. Zheng, B. D. Ratner, S. Jiang, *J. Phys. Chem. B* **2005**, *109*, 2934.
- [42] M.-C. Sin, S.-H. Chen, Y. Chang, *Polym. J.* **2014**, *46*, 436.
- [43] C. Rodriguez-Emmenegger, M. Houska, A. B. Alles, E. Brynda, *Macromol. Biosci.* **2012**, *12*, 1413.
- [44] A. de los Santos Pereira, S. Sheikh, C. Blaszykowski, O. Pop-Georgievski, K. Fedorov, M. Thompson, C. Rodriguez-Emmenegger, *Biomacromolecules* **2016**, *17*, 1179.
- [45] Z. Wu, H. Chen, X. Liu, Y. Zhang, D. Li, H. Huang, *Langmuir* **2009**, *25*, 2900.
- [46] G. Cheng, G. Li, H. Xue, S. Chen, J. D. Bryers, S. Jiang, *Biomaterials* **2009**, *30*, 5234.
- [47] F. Obstals, M. Vorobii, T. Riedel, A. de Los Santos Pereira, M. Bruns, S. Singh, C. Rodriguez-Emmenegger, *Macromol. Biosci.* **2018**, *18*, 1700359.
- [48] C. Leng, X. Han, Q. Shao, Y. Zhu, Y. Li, S. Jiang, Z. Chen, *J. Phys. Chem. C* **2014**, *118*, 15840.
- [49] Q. Shao, S. Jiang, *Adv. Mater.* **2015**, *27*, 15.
- [50] C. Leng, S. Sun, K. Zhang, S. Jiang, Z. Chen, *Acta Biomater.* **2016**, *40*, 6.
- [51] C. A. Del Grosso, C. Leng, K. Zhang, H.-C. Hung, S. Jiang, Z. Chen, J. J. Wilker, *Chem. Sci.* **2020**, *11*, 10367.
- [52] J. Kopeček, H. Bažilová, *Eur. Polym. J.* **1973**, *9*, 7.
- [53] K. R. Whiteman, V. Subr, K. Ulbrich, V. P. Torchilin, *J. Liposome Res.* **2001**, *11*, 153.
- [54] S. G. Krimmer, H. Pan, J. Liu, J. Yang, J. Kopecek, *Macromol. Biosci.* **2011**, *11*, 1041.
- [55] A. Kelsch, S. Tomcin, K. Rausch, M. Barz, V. Mailänder, M. Schmidt, K. Landfester, R. Zentel, *Biomacromolecules* **2012**, *13*, 4179.
- [56] L. Nuhn, M. Barz, R. Zentel, *Macromol. Biosci.* **2014**, *14*, 607.
- [57] F. A. de Oliveira, L. J. C. Albuquerque, K. A. Riske, E. Jager, F. C. Giacomelli, *J. Colloid Interface Sci.* **2020**, *574*, 260.
- [58] M. Vorobii, A. de los Santos Pereira, O. Pop-Georgievski, N. Y. Kostina, C. Rodriguez-Emmenegger, V. Percec, *Polym. Chem.* **2015**, *6*, 4210.
- [59] A. R. Kuzmyn, A. T. Nguyen, L. W. Teunissen, H. Zuilhof, J. Baggerman, *Langmuir* **2020**, *36*, 4439.
- [60] E. Roeven, A. R. Kuzmyn, L. Scheres, J. Baggerman, M. M. J. Smulders, H. Zuilhof, *Langmuir* **2020**, *36*, 10187.
- [61] C. Rodriguez-Emmenegger, S. Janel, A. de los Santos Pereira, M. Bruns, F. Lafont, *Polym. Chem.* **2015**, *6*, 5740.
- [62] C. J. Van Oss, M. K. Chaudhury, R. J. Good, *Chem. Rev.* **1988**, *88*, 927.
- [63] B. Lopez-Mila, P. Alves, T. Riedel, B. Dittrich, F. Mergulhao, C. Rodriguez-Emmenegger, *Bioinspir. Biomim.* **2018**, *13*, 065001.
- [64] C. Rodriguez-Emmenegger, O. Kylian, M. Houska, E. Brynda, A. Artemenko, J. Kousal, A. B. Alles, H. Biederman, *Biomacromolecules* **2011**, *12*, 1058.

- [65] C. Rodriguez-Emmenegger, C. M. Preuss, B. Yameen, O. Pop-Georgievski, M. Bachmann, J. O. Mueller, M. Bruns, A. S. Goldmann, M. Bastmeyer, C. Barner-Kowollik, *Adv. Mater.* **2013**, 25, 6123.
- [66] O. Pop-Georgievski, C. Rodriguez-Emmenegger, A. L. S. Pereira, V. Proks, E. Brynda, F. Rypacek, *J. Mater. Chem. B* **2013**, 1, 2859.
- [67] X. Fan, L. Lin, J. L. Dalsin, P. B. Messersmith, *J. Am. Chem. Soc.* **2005**, 127, 15843.
- [68] M. Dahm, B. J. Chang, O. Prucker, M. Pierkes, T. Alt, E. Mayer, J. Ruhe, H. Oelert, *Ann. Thorac. Surg.* **2001**, 71, S437.
- [69] O. Sterner, A. Serrano, S. Mieszkin, S. Zurcher, S. Tosatti, M. E. Callow, J. A. Callow, N. D. Spencer, *Langmuir* **2013**, 29, 13031.
- [70] D. Knoll, J. Hermans, *J. Biol. Chem.* **1983**, 258, 5710.
- [71] K. Holmberg, F. Tiberg, M. Malmsten, C. Brink, *Colloids Surf., A* **1997**, 123–124, 297.
- [72] E. P. Currie, W. Norde, M. A. Cohen Stuart, *Adv. Colloid Interface Sci.* **2003**, 100–102, 205.
- [73] P. Uhlmann, H. Merlitz, J. U. Sommer, M. Stamm, *Macromol. Rapid Commun.* **2009**, 30, 732.
- [74] S. Zurcher, D. Wackerlin, Y. Bethuel, B. Malisova, M. Textor, S. Tosatti, K. Gademann, *J. Am. Chem. Soc.* **2006**, 128, 1064.
- [75] S. Dedisch, F. Obstals, A. los Santos Pereira, M. Bruns, F. Jakob, U. Schwaneberg, C. Rodriguez-Emmenegger, *Adv. Mater. Interfaces* **2019**, 6, 1900847.
- [76] W. Gong, J. Wang, Z. Chen, B. Xia, G. Lu, *Biochemistry* **2011**, 50, 3621.
- [77] R. A. Meurer, S. Kemper, S. Knopp, T. Eichert, F. Jakob, H. E. Goldbach, U. Schwaneberg, A. Pich, *Angew. Chem., Int. Ed. Engl.* **2017**, 56, 7380.
- [78] P. Schwinges, S. Pariyar, F. Jakob, M. Rahimi, L. Apitius, M. Hunsche, L. Schmitt, G. Noga, C. Langenbach, U. Schwaneberg, U. Conrath, *Green Chem.* **2019**, 21, 2316.
- [79] S. Dedisch, A. Wiens, M. D. Davari, D. Söder, C. Rodriguez-Emmenegger, F. Jakob, U. Schwaneberg, *Biotechnol. Bioeng.* **2020**, 117, 49.
- [80] K. Rübsam, B. Stomps, A. Boker, F. Jakob, U. Schwaneberg, *Polymer* **2017**, 116, 124.
- [81] K. Rübsam, L. Weber, F. Jakob, U. Schwaneberg, *Biotechnol. Bioeng.* **2018**, 115, 321.
- [82] K. Rubsam, M. D. Davari, F. Jakob, U. Schwaneberg, *Polymers* **2018**, 10, 423.
- [83] M. Noth, Z. Zou, I. El-Awaad, L. C. de Lencastre Novaes, G. Dilarri, M. D. Davari, H. Ferreira, F. Jakob, U. Schwaneberg, *Biotechnol. Bioeng.* **2021**, 118, 1520.
- [84] V. Percec, T. Guliasvili, J. S. Ladislaw, A. Wistrand, A. Stjern Dahl, M. J. Sienkowska, M. J. Monteiro, S. Sahoo, *J. Am. Chem. Soc.* **2006**, 128, 14156.
- [85] B. M. Rosen, V. Percec, *Chem. Rev.* **2009**, 109, 5069.
- [86] N. Zhang, S. R. Samanta, B. M. Rosen, V. Percec, *Chem. Rev.* **2014**, 114, 5848.
- [87] G. Lligadas, S. Grama, V. Percec, *Biomacromolecules* **2017**, 18, 1039.
- [88] G. Lligadas, S. Grama, V. Percec, *Biomacromolecules* **2017**, 18, 2981.
- [89] X. Feng, D. S. Maurya, N. Bensabeh, A. Moreno, T. Oh, Y. Luo, J. N. Lejniaks, M. Galià, Y. Miura, M. J. Monteiro, *Biomacromolecules* **2020**, 21, 250.
- [90] D. S. Maurya, A. Malik, X. Feng, N. Bensabeh, G. Lligadas, V. Percec, *Biomacromolecules* **2020**, 21, 1902.
- [91] A. Royant, M. Noirclerc-Savoie, *J. Struct. Biol.* **2011**, 174, 385.
- [92] N. H. Nguyen, C. Rodriguez-Emmenegger, E. Brynda, Z. Sedlakova, V. Percec, *Polym. Chem.* **2013**, 4, 2424.
- [93] N. H. Nguyen, V. Percec, *J. Polym. Sci., Part A: Polym. Chem.* **2010**, 48, 5109.
- [94] N. H. Nguyen, J. Kulis, H.-J. Sun, Z. Jia, B. van Beusekom, M. E. Levere, D. A. Wilson, M. J. Monteiro, V. Percec, *Polym. Chem.* **2013**, 4, 144.
- [95] M. Kaba, N. Raklaoui, M. F. Guimon, A. Mas, *J. Appl. Polym. Sci.* **2005**, 97, 2088.
- [96] R. A. Latour, *J. Biomed. Mater. Res., Part A* **2015**, 103, 949.
- [97] A. Savara, C. M. Schmidt, F. M. Geiger, E. Weitz, *J. Phys. Chem. C* **2009**, 113, 2806.
- [98] N. M. Green, *Avidin*, Academic Press, New York **1975**.
- [99] L. G. Parratt, *Phys. Rev.* **1954**, 95, 359.
- [100] H. Ma, M. Wells, T. P. Beebe, A. Chilkoti, *Adv. Funct. Mater.* **2006**, 16, 640.
- [101] E. van Andel, S. C. Lange, S. P. Pujari, E. J. Tijhaar, M. M. J. Smulders, H. F. J. Savelkoul, H. Zuilhof, *Langmuir* **2019**, 35, 1181.
- [102] J. G. Archambault, J. L. Brash, *Colloids Surf., B* **2004**, 39, 9.
- [103] J. Groll, Z. Ademovic, T. Ameringer, D. Klee, M. Moeller, *Biomacromolecules* **2005**, 6, 956.
- [104] A. Wörz, B. Berchtold, K. Moosmann, O. Prucker, J. Ruhe, *J. Mater. Chem.* **2012**, 22, 19547.
- [105] P. Saha, M. Santi, M. Emondts, H. Roth, K. Rahimi, J. Grosskurth, R. Ganguly, M. Wessling, N. K. Singha, A. Pich, *ACS Appl. Mater. Interfaces* **2020**, 12, 58223.